



# Moving-Press: Pressure-based Moving Phantom Sensation for Immersive VR Hand Interaction

DONGKYU KWAK\*, Graduate School of Culture Technology, KAIST, Republic of Korea

KYUNGJIN SEO\*, Graduate School of Culture Technology, KAIST, Republic of Korea

RACHEL KIM, School of Computing, KAIST, Republic of Korea

SANG HO YOON, Graduate School of Culture Technology, KAIST, Republic of Korea

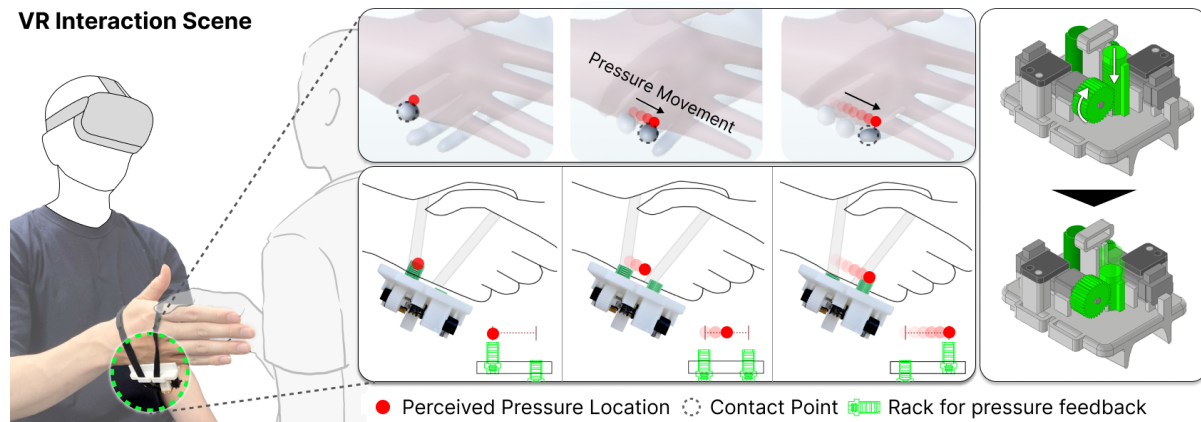


Fig. 1. Moving-Press enables pressure movement feedback in VR. In the VR handshake scenarios, interaction accompanied the pressure movement on the user's hand. To do so, we varied the indentation depth of two actuators to change the perceived location of pressure feedback. We used a rack-and-pinion mechanism to render pressure feedback.

We propose a haptic interface, Moving-Press, enabling a pressure-based moving phantom sensation on the user's hand. The moving phantom sensation refers to an illusory perception of a continuous tactile stimulus traversing between two discrete stimulation points. While this phenomenon has been studied in the context of vibrotactile feedback, it remains underexplored in the domain of pressure feedback. As integrating phantom sensation offers a promising approach to simplifying typically bulky pressure devices, employing this phenomenon enables more compact pressure rendering systems. Therefore, we investigated whether pressure movement could be induced using two fixed-positioned actuators by leveraging pressure-based phantom sensation. Our initial perception study validated the occurrence of pressure-based phantom sensations on the hand. Then, we examined how varying the indentation depth of each actuator influences the perceived location, and how the phantom sensation intensity differs from a single pressure stimulus. Finally, we proposed a rack-and-pinion-driven wearable

\*Both authors contributed equally to this research.

Authors' Contact Information: DongKyu Kwak, kig160@kaist.ac.kr, Graduate School of Culture Technology, KAIST, Daejeon, Republic of Korea; Kyungjin Seo, kjseo@kaist.ac.kr, Graduate School of Culture Technology, KAIST, Daejeon, Republic of Korea; Rachel Kim, School of Computing, KAIST, Daejeon, Republic of Korea, rachel02@kaist.ac.kr; Sang Ho Yoon, Graduate School of Culture Technology, KAIST, Daejeon, Republic of Korea, sangho@kaist.ac.kr.



This work is licensed under a Creative Commons Attribution 4.0 International License.

© 2025 Copyright held by the owner/author(s).

ACM 2474-9567/2025/12-ART185

<https://doi.org/10.1145/3770682>

haptic device and conducted a user study to identify an appropriate haptic rendering profile for producing natural pressure movement. The results demonstrated that temporal modulation of indentation depth using the proposed device successfully evokes pressure-based moving phantom sensation.

**CCS Concepts:** • **Human-centered computing** → **Haptic devices; Human computer interaction (HCI); User studies; Virtual reality.**

**Additional Key Words and Phrases:** pressure feedback, tactile illusion, wearables, haptics

**ACM Reference Format:**

DongKyu Kwak, Kyungjin Seo, Rachel Kim, and Sang Ho Yoon. 2025. Moving-Press: Pressure-based Moving Phantom Sensation for Immersive VR Hand Interaction. *Proc. ACM Interact. Mob. Wearable Ubiquitous Technol.* 9, 4, Article 185 (December 2025), 24 pages. <https://doi.org/10.1145/3770682>

## 1 INTRODUCTION

In virtual reality (VR), users frequently encounter touch when interacting with external environments. Touch plays a crucial role in conveying information about virtual objects and enables emotional interactions with others [3, 18]. Touch allows users to perceive the shape of virtual objects, manipulate them, or even foster social or emotional connections, such as stroking another user’s arm or shaking hands with the other person’s avatar. For an immersive experience in these scenarios, users anticipate a smooth movement of pressure on their hands. Thus, implementing realistic pressure movement enriches embodied interactions in virtual reality.

However, delivering realistic pressure feedback through haptic devices typically leads to a bulky and heavy form factor [6, 22, 33]. The addition of mechanical structures requires users to wear a device of substantial size and weight, which increases user fatigue. To achieve a more compact actuator structure, researchers have designed the pin array devices, which reduced the actuators’ size while increasing their number to provide realistic feedback [4, 69]. Nevertheless, these remain bulky and unsuitable for wearable applications since each actuator only provides sensation at a fixed point.

To address this, a haptic device should evoke sensation in regions without actuators, thereby reducing the number of actuators while expanding the haptic rendering area. This study leverages a tactile illusion, specifically phantom sensation, to enable the pressure feedback in locations without actuators. Phantom sensation refers to an illusory tactile sensation perceived midway between two actuators [42]. Previous studies have employed this illusion to achieve realistic feedback with fewer actuators, particularly in vibrotactile rendering [42, 70]. In this study, we extend this approach to pressure feedback, enabling pressure sensations at unactuated regions.

Phantom sensation covers a large rendering area with only a few actuators, yet the research remains heavily weighted toward vibration rather than pressure [28–30, 50]. Indeed, vibrotactile phantom sensation has advanced toward moving phantom sensation [8, 70] and a rendering formula [19, 42, 56] for realistic sensation. However, given that human mechanoreceptors for vibration and pressure differ [23, 46], prior knowledge from vibrotactile feedback cannot be directly applied to pressure feedback. Therefore, research on pressure-based phantom sensation should be explored.

There are only a few studies that apply tactile illusion on pressure feedback [11, 17, 66]. A recent study demonstrated the pressure movement using pneumatic actuators [17]. Still, they did not investigate a moving phantom sensation or explore their application on the hand, where most interactions occur. Here, we aim to validate the feasibility of pressure-based moving phantom sensation on the hand, specifically the ulnar-sided hand. To address this, we defined two research questions.

**RQ1:** Can we induce pressure-based phantom sensation on the hand?

**RQ2:** Can we induce pressure-based moving phantom sensation on the hand?

Given the limited studies applying pressure-based phantom sensation to the hand, we defined the research question for a systematic investigation of this phenomenon. Since distinct receptors underlie pressure and vibration,

Table 1. Comparison of existing pressure devices. Our device renders localized pressure and pressure movement on the ulnar-sided hand while allowing free hand movement with a lightweight design.

Device	Contact Location	Pressure Type	Pressure Movement	Free Hand	Weight (g)	Normal Force (N)
Tasbi [45]	Wrist	Distributed	✗	-	200	12
Aggravi et al. [1]	Forearm	Distributed	✗	-	220	10
Henell et al. [17]	Forearm	Distributed	✓	-	68	4.0
Deltatouch [60]	Hand (Palm)	Localized	✓	✗	30	4.2
HapticSpider [33]	Hand (Palm)	Localized	✓	✗	450	6.0
<b>Our</b>	Hand (Ulnar-Sided)	Localized	✓	✓	50	6.0

we used a phased methodology rather than directly applying vibrotactile methods. To answer the **RQ1**, we investigated the occurrence of phantom sensation (*Perception Study 1*), location of phantom sensation (*Perception Study 2*), and intensity of phantom sensation (*Perception Study 3*). After verifying **RQ1**, we proceeded to examine our primary research goal (**RQ2**). We developed a rack-and-pinion-driven wearable haptic device and validated the rendering method for a more natural pressure movement experience (*User Study*).

Our work not only examines the perceptual traits of pressure-based phantom sensation but also incorporates the findings into our newly designed haptic device. The main contributions of the paper are as follows:

- We identified the key perceptual features of pressure-based phantom sensation on the hand, including occurrence distance, perceived location, and perceived intensity.
- We proposed a novel rack-and-pinion-driven wearable haptic device that renders pressure movement.
- We implemented a pressure-based moving phantom sensation and validated the appropriate rendering method through a user study.

## 2 RELATED WORK

### 2.1 Pressure-based Haptic Feedback

To replicate the realistic sense of touch in VR, researchers have developed numerous pressure feedback devices, including motor-based systems [45, 68], pneumatic devices [12, 16, 71], and soft materials [54, 55]. To provide precise pressure feedback in a wearable form factor, researchers should design a device that is compact and capable of precise force control. Motor-based actuators usually ensure non-backdrivability, allowing precise device control without deformation under substantial forces. However, they typically suffer from bulky form factors [32]. Pneumatic and soft materials suggest compact form factors, but their deformability under minimal force prevents precise control [37, 55]. Additionally, these mechanical and pneumatic devices typically provide stimulation only at fixed locations with a single actuator. Thus, the only solution for increasing the rendering area is to increase the number of actuators.

Moreover, previous pressure-based haptic devices typically applied pressure around the entire circumference of the arm [1, 45, 68]. Whereas devices targeting the hand [13, 32, 33, 60] often restrict finger mobility. Furthermore, previous devices moved the actuator to render pressure movement, which caused mechanical instability due to undesired vibrations. In contrast, our device is mounted on the ulnar-sided hand to maintain natural finger mobility. By leveraging phantom sensation to simulate pressure movement, the actuators remain stationary, resulting in improved stability and a more secure fit (Table 1).

In this work, we drew inspiration from conventional pin-array devices [4, 20, 69] to formulate a mechanism capable of delivering localized pressure feedback. We designed the device using a rack-and-pinion structure that transmits vertical indentation towards the skin. Rather than applying pressure around the circumference of the arm [45], our system applies pressure to a localized region, providing a more realistic sensation in such scenarios.

## 2.2 Tactile Illusion for Movement Sensation

Tactile feedback enriches the information transfer [14, 42]. However, designing the haptic device that faithfully reproduces the sensation of real-object touch remains technically challenging. To address this, researchers have explored the tactile illusions as a means to render feedback with fewer actuators. These tactile illusions also evoke the tactile movement through temporal modulation of actuator outputs. Moving phantom sensation refers to the user's perception of two distinct stimuli as a single moving stimulus at a midway point of multiple actuators [8, 70]. Apparent tactile motion simulates the movement of a stimulus by overlapping actuation times and varying the amplitude continuously [7, 52]. Among the various tactile illusion methods, we especially focus on the moving phantom sensation, as amplitude-modulated phantom sensation yields more salient tactile perception [2].

Previously, researchers have predominantly studied the moving phantom sensations for the vibrotactile feedback [19, 29, 48, 70], not for the pressure feedback. Because pressure feedback devices require more complex structures than vibrotactile ones, tactile illusion techniques can be more effectively applied. However, we cannot directly apply the rendering method identified in vibrotactile studies, as the receptors for pressure and vibration are distinct [17, 23, 46].

A few studies demonstrated the pressure movement using apparent motion with pneumatic actuators [17, 66]. However, they didn't employ the amplitude variation approach, and they conducted the experiments on the forearm rather than on the hand, where the most interactions occur. Here, we investigated that varying the indentation depths of two actuators can evoke the pressure-based phantom sensation on the user's hand.

## 3 DESIGN RATIONALE FOR PRESSURE-BASED MOVING PHANTOM SENSATION

Realistic pressure movement sensation during touch interaction improves the immersiveness in VR experiences. Instead of relying only on bulky, multi-actuator systems, we leverage the phantom sensation to simulate pressure movement with a simplified device design. To this end, we investigate the perceptual characteristics of pressure-based moving phantom sensation and present a wearable device that provides pressure feedback. By combining these elements, we introduce Moving-Press, a novel haptic interface. In this session, we present the rationale behind key design parameters necessary for rendering pressure feedback.

### 3.1 Choosing Hand Region for Pressure Feedback

In this paper, we chose the hypothenar region of the palm for delivering pressure feedback. Specifically, we applied pressure feedback along the ulnar border of the hand [25], which we refer to as the ulnar-sided hand (USH).

We first aimed to render pressure movement on the hand surface. Prior research [63] has demonstrated that two discrete pressure stimuli are merged in the metacarpophalangeal (MCP) joint region of the palm, forming a single perceived sensation. Therefore, we chose the palm as a good candidate to apply pressure-based phantom sensation. Within the palm, we specifically chose the hypothenar region because its broad and thick surface provides a stable base for attaching the device. A commercial device [49] also stimulates the hypothenar region as part of delivering pressure feedback to the entire palm.

Another reason that we chose the hand as a target region is that the hand plays a central role in social interactions, particularly in virtual meeting scenarios. One of the most representative gestures is the handshake, which serves as a medium for first impressions [9] and a foundation for further interaction. The USH is the primary area of firm contact during a handshake [59]. Because USH receives direct contact from the opponent's actively moving fingers, this area experiences a high degree of contact variability. Previous haptic devices [59, 64, 67] for handshake have yet to achieve dynamic movement of pressure. Our device applies pressure to the target area using a rack-and-pinion mechanism and integrates phantom sensation to render the perception of pressure movement. Placing the device on the USH allows the fingers to move freely, which enhances usability and enables

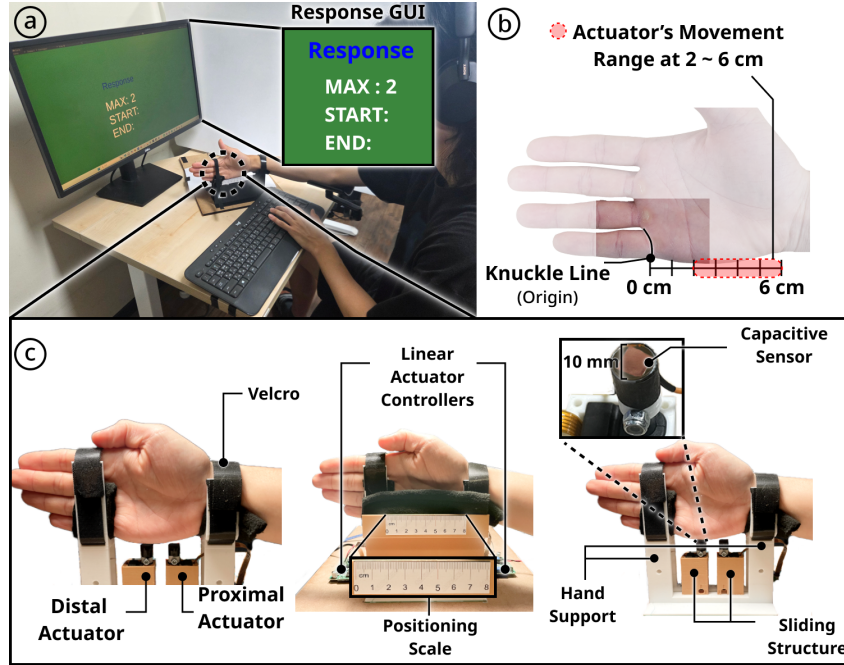


Fig. 2. Perception study setup. (a) Study environment with a response GUI. (b) We define the knuckle line as the origin for initial positioning. The actuator operates within a 2 ~ 6 cm range to avoid the MCP joint (c). Distal and proximal actuators for pressure feedback. Users place their hands on the hand support, and we employ a capacitive sensor to calibrate the initial contact point between the actuator and the skin.

easy integration with other hand-mounted devices. This configuration enhances the immersiveness of hand-based haptic interaction.

### 3.2 Contact Area Size of Pressure Feedback

Previous work showed that tactile stimuli with a diameter of 1 mm or greater can be perceived as a single stimulus [61], and another study employed a 15 mm actuator diameter on the forearm [31]. Given that tactile acuity on the palm is higher than on the forearm [24, 62], we applied the actuator diameter to 10 mm (Figure 2c). In this study, we used a 10 mm diameter actuator to deliver pressure feedback, defining that indentation depth is the displacement of the actuator after making contact with the skin. To do so, we performed a calibration procedure using capacitive sensors to measure the contact point whenever the user's hand position changed during the perception study (Figure 2c).

## 4 PERCEPTION STUDY

We conducted three perception studies to validate our research question. The experimental setup and detailed procedures are presented below. Participants were paid \$10 following an IRB-approved study.

### 4.1 Study Setup

We designed a grounded experimental device (Figure 2c) for use in the three perception studies. The device delivers pressure feedback by rendering a target indentation depth at a specified location on the USH. The device

applies pressure using a linear actuator (Actuonix PQ12-P) with 10 mm diameter. We installed two linear actuators, one positioned proximally and the other distally along the USH. For two-point stimuli, both actuators were activated simultaneously. For a one-point stimulus, only the actuator closest to the target location was activated. The sliding structure allowed each actuator to be positioned precisely along the USH. The hand support and sliding structure were fabricated using a 3D printer (PLA material), and a velcro strap was used to secure the user's hand during the experiment.

Once participants placed their right hand on the support and fastened the velcro strap, the actuators were positioned using the sliding mechanism and operated through linear actuator controllers to deliver the pressure feedback. The system was controlled via an Arduino Mega (ATmega2560) microcontroller connected to a PC through serial communication. The linear actuator provided a maximum stroke of 20 mm from its origin.

To ensure accurate detection of the initial skin contact point, we performed a calibration procedure. A capacitive sensor (MPR121) was attached to the tip of the linear actuator to detect the moment of contact. We first measured the distance from the actuator's origin to the contact point on the skin. The final activation height of the actuator was then determined by adding the target indentation depth to the calibrated contact point, allowing precise delivery of the intended pressure feedback.

## 4.2 Perception Study 1: Actuators Spacing Threshold on the Hand

**4.2.1 Methods.** To investigate **RQ1**, it is essential to determine the maximum distance between actuators that can reliably induce pressure-based phantom sensation. When two actuators are placed too closely, users may perceive a single unified sensation, but this reduces the pressure rendering range. Conversely, if two actuators are too far apart, users are likely to perceive two distinct stimuli rather than evoking a phantom sensation. Therefore, we examine the maximum actuator spacing required to induce pressure-based phantom sensation on USH. Given the limited prior research on pressure-based phantom sensation on the hand, our goal was to establish its quantitative characteristics. We used the grounded experimental device for this study (Figure 2c).

**Study Setup** We recruited 18 participants (7 female,  $25 \pm 3.45$  years old) for the experiment. All participants provided written informed consent before the experiment. In this study, participants received pressure feedback on either a one-point stimulus with a single linear actuator or two-point stimuli with two linear actuators. To determine the pressure rendering area along the USH, we defined the knuckle line near the pinky MCP joint as the origin (0 cm) point (Figure 2b). We established a consistent origin as a pinky knuckle line across all participants. The actuator's movement range is 2 ~ 6 cm, with a total of 4 cm movement range. We applied a 2 cm offset to avoid direct pressure on the MCP joint because of its hardness. Additionally, we set the maximum range to 6 cm to accommodate across various users [21]. We positioned each actuator at 9 different locations (2, 2.5, 3, 3.5, 4, 4.5, 5, 5.5, and 6 cm). We divided the 4 cm pressure rendering range into 0.5 cm resolution intervals. For two-point stimuli conditions, the minimum distance between two actuators is set to 1.5 cm, considering previous findings that summation of pressure feedback by small tips on the palm occurs around 2.5 cm [63].

To determine how users' perception varies for different indentation depths, we conducted the study under two different amounts of indentation depth, 4 mm and 8 mm, respectively. Given users' pressure sensitivity [47] and the 12 mm indentation depth range availability [44], we evenly divided this range to define the experimental variables. In the 8 mm condition, we raised a single actuator by 8 mm for a one-point stimulus, whereas for two-point stimuli, both actuators were raised by 4 mm each. We completely randomized the experimental conditions. We carried out a total of 78 trials (2 indentation depths  $\times$  (9 one-point stimulus  $\times$  2 repetitions + 21 two-point stimuli)) per participant.

**Procedure** After a short briefing about the study and calibration session, participants carried out the main session, which was conducted within an hour. During the calibration session, we recorded the height required to

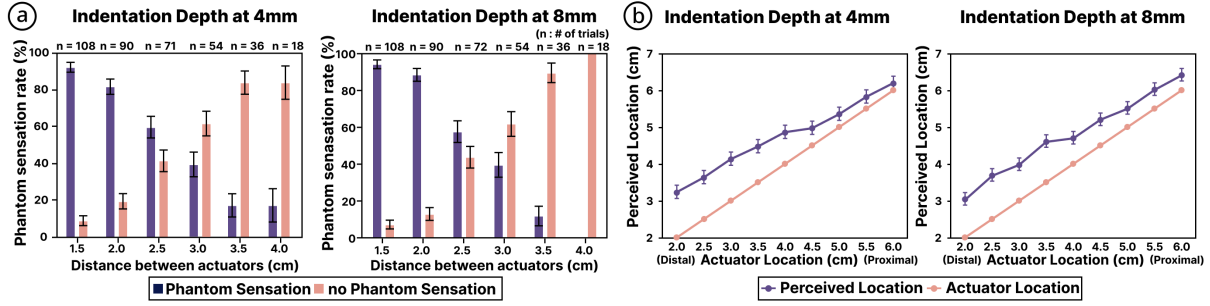


Fig. 3. Results of Perception Study 1. (a) The phantom sensation occurrence rate by the distance between two actuators for the two-point stimuli condition. (b) The localization error of a one-point stimulus. Error bars indicate standard error.

reach the USH at each location. If the calibration height was 4 mm and the desired actuation depths were 4 mm, the actuator moved a total of 8 mm

In this study, we randomly stimulated participants with one-point or two-point stimuli along the USH while users didn't know the stimulus type. After each trial, we asked participants to report the number of perceived stimuli and their perceived locations. After each trial, participants reported the number of perceived stimuli and their locations by entering them using a keyboard. To indicate the location, they used a positioning scale (Figure 2c) with 0.1 cm resolution attached to the ground device. Here, if users perceived two-point stimuli as a single sensation, it means that pressure-based phantom sensation occurred on the USH.

**4.2.2 Results.** Figure 3a illustrates the occurrence of pressure-based phantom sensation by a distance of two actuators for the two-point stimuli condition. If participants perceived the two-point stimuli as a single sensation, it indicated that phantom sensations occurred (navy bar in Figure 3a). Conversely, if they distinguished them as two distinct points, the phantom sensation did not occur (pink bar in Figure 3a). At both 4 mm and 8 mm indentation depth, the threshold at which more than 50 % of users feel the phantom sensation is 2.5 cm, and more than 80% did so when the distance was within 2 cm.

Figure 3b shows the localization error between the actual location of the actuator and the perceived location for the one-point stimulus. Overall, the perceived location was biased in the positive direction relative to the actual location, indicating that users tended to perceive the stimulus proximally. Across all the trials, the mean of localization error was approximately 0.76 cm. We conducted a statistical analysis to investigate the difference in localization error between 4 mm and 8 mm conditions. Since the Shapiro-Wilk test indicated a normality for the given data ( $p=0.086$ ), we proceeded with a paired t-test and found no significant difference between the groups ( $t=1.53$ ,  $p=0.15$ ).

Table 2 summarizes the perceived location when phantom sensation occurred. We excluded the groups with fewer than 10 data points. It was observed that the user's perceived location was slightly biased in the positive direction (proximal) compared to the midpoint between the two actuators, similar to the one-point stimulus. Likewise, we conducted a statistical analysis to investigate the difference between 4 mm and 8 mm conditions. Since the Shapiro-Wilk test indicated a normality for the given data ( $p=.46$ ), we conducted a paired t-test and found that there is no significant difference between both 4 mm and 8 mm groups ( $t=1.43$ ,  $p=0.17$ ). In this phantom sensation condition, the target location was defined as the middle of the two stimulated actuator positions. We found the perceived location of two-point stimuli is biased 0.59 cm toward the proximal direction.

**4.2.3 Discussion.** The study results confirm that pressure-based phantom sensation is induced on the USH. We employed a two-actuator spacing of 2 cm in the subsequent development of our wearable haptic device. We set

Table 2. Perceived location (mean value w/SD) by actuator locations and different indentation depth levels. PS (%) indicates the proportion of participants reporting phantom sensations. Perceived locations are proximally biased compared to the midpoint of two actuators (\*). Rows with fewer than 10 data points were removed.

Two Actuator Locations (cm, cm)	Indentation Depth			
	4 mm		8 mm	
	PS (%)	Perceived location (cm)	PS (%)	Perceived location (cm)
(2.0, 3.5)	88.9	3.8(1.3)*	88.9	3.6(1.0)
(2.0, 4.0)	94.4	4.2(1.1)	72.2	3.8(1.2)
(2.0, 4.5)	77.8	4.1(1.1)	61.1	4.1(1.3)
(2.5, 4.0)	100.0	4.3(1.1)	83.3	4.0(1.3)
(2.5, 4.5)	88.9	4.2(1.1)	77.8	4.4(1.2)
(2.5, 5.0)	–	–	66.7	4.5(0.9)
(3.0, 4.5)	94.4	4.3(1.2)	94.4	4.3(1.3)
(3.0, 5.0)	88.9	4.3(0.9)	94.4	4.9(1.4)
(3.0, 5.5)	61.1	4.9(0.9)	55.6	4.4(0.6)
(3.5, 5.0)	100.0	4.7(1.0)	100.0	4.9(0.9)
(3.5, 5.5)	88.9	5.1(0.9)	88.9	5.1(1.2)
(4.0, 5.5)	88.9	4.9(1.0)	88.9	5.1(1.0)
(4.0, 6.0)	77.8	5.3(1.0)	72.2	5.3(1.0)
(4.5, 6.0)	88.9	5.8(1.0)	94.4	5.5(1.0)

the 80 % threshold for robustly evoking the phantom sensation, considering the higher sensitivity of the hand compared to other body regions [58].

An interesting finding is that the perceived location of pressure feedback reported by users exhibited a proximal bias both for the one-point and the two-point stimuli. While it was intuitively expected that users would perceive the location at the midpoint between two actuators when we drive two actuators at equal indentation depth, the results revealed a bias in perceived location. An average proximal bias is 0.76 cm for the one-point stimulus and 0.59 cm for the two-point stimuli. This bias is also reported in other body parts [17, 27], and an explanation for this phenomenon is by an anchor point effect [65], whereby the user's perception is affected by an anatomical reference point. In our experiments, the wrist appears to serve this role, which is reported in earlier research [10]. As a result, users perceived the stimulus as biased toward the wrist.

Additionally, we investigated how perceptual characteristics change with different indentation depths. Because the actuator maximum distance for phantom sensation and the perceived location for one-point and two-point stimuli are the same in both the 4 mm and 8 mm conditions, we conclude that the user's perceptual traits do not depend on the amount of indentation depth for 4 mm and 8 mm cases.

### 4.3 Perception Study 2: Effect of Varying Indentation Depths on Perceived Location

**4.3.1 Methods.** *Perception Study 1* demonstrated that pressure-based phantom sensation can be successfully induced on the USH. Building on this result, we designed a follow-up experiment to investigate whether the perceived location of the stimulus shifts by varying the indentation depth of the two actuators. In contrast to the previous study, where both actuators were driven at the same indentation depth, the current study varied their depths to investigate how this manipulation influences the perceived location. We used the same device as in *Perception Study 1*.

**Study Setup** We recruited 18 participants (7 female,  $25.8 \pm 4.3$  years old) for the experiment. All participants were provided written informed consent before the experiment. For the experimental setup, we defined the indentation ratio, which represents the indentation depth by proximal actuator (Figure 2c) divided by the total indentation depth of two actuators. The ratio can vary between 0 and 1. A value of 0 indicates that the total amount of indentation depth is entirely allocated toward the distal actuator, whereas a value of 1 is allocated toward the proximal actuator. We investigate whether different ratios could induce a shift in the perceived location. Based on a pilot study that revealed a sigmoid-like relationship between indentation ratio and perceived location, we selected seven indentation ratios (0, 0.3, 0.4, 0.5, 0.6, 0.7, and 1) to densely sample the middle range to capture this sigmoid perceptual trend.

Since we validated that pressure-based phantom sensation occurs within the 2 cm spacing of two actuators, the distance between the two actuators was fixed as 2 cm. The distal actuator was placed at three different positions, 2 cm, 3 cm, and 4 cm in figure 2b. Accordingly, the proximal actuator was positioned at 4 cm, 5 cm, and 6 cm.

To investigate the perceptual effect from different indentation depths, we set the total amount of indentation depth into 7 different conditions (4, 5, 6, 7, 8, 9, 10 mm). This design allowed us to investigate how the perceived location varies with the size of the indentation depth. Each distal actuator location was treated as an experimental block where both the indentation ratio and indentation depth were fully randomized, and the sequence of blocks was counterbalanced using a Latin square design. Considering the 3 distal actuators' locations and two repetitions, each participant completed a total of six blocks. The overall number of trials was 294 trials (7 indentation ratios  $\times$  3 different actuator positions  $\times$  7 different indentation depths  $\times$  2 repetitions). After each trial, participants reported the perceived location, and if the sensation was felt as a spatially extended range, they indicated both the start and end points of the interval. Even when the stimulus was perceived as an interval, we collected a single perceived location, as users are capable of identifying a local maximum even when the stimulus spread laterally [61]. This approach enabled us to estimate the most prominent point of perception under realistic conditions where the wearable device is implemented with a 2 cm actuator spacing.

**Procedure** Participants received a brief explanation of the study and completed a calibration step identical to that in Perception Study 1. After a minute of practice sessions involving example stimuli, participants proceeded to the main experiment. We offered a 1-minute break whenever the distal actuator location changed, where the calibration step was repeated. During each trial, participants reported the perceived location of the pressure feedback using a keyboard and a positioning scale (Figure 2c) and proceeded to the next trial by pressing the spacebar. The entire experiment lasted about an hour.

**4.3.2 Results.** Figure 4 shows the perceived location across seven indentation ratios and seven different indentation depths. As the ratio increased from 0 to 1, the perceived location shifted proximally as we expected. Additionally, we observed a tendency for greater indentation depth to result in a more distal perceived location. When the distal actuator is located at 2 cm, users' average range of perceived location was 2.9 cm to 4.0 cm. When it is located at 3 cm, users' average response range is 3.7 cm to 5.2 cm. When it is located at 4 cm, users' average response range is 4.6 cm to 6.0 cm (Table 3). For the statistical analysis, we applied ART ANOVA to assess the effects of indentation depth and indentation ratio at each actuator position since the data show non-normality with the Shapiro-Wilk test. Subsequently, Wilcoxon signed-rank tests with Bonferroni correction were conducted as post-hoc analyses.

At the distal actuator position located at 2 cm, a significant main effect was found for both indentation depth and indentation ratio ( $F(6, 102) = 4.0, p < .001$  and  $F(6, 102) = 87.9, p < .001$ ). No significant interaction effect was observed. Post-hoc analyses revealed that the 4 mm indentation depth differed significantly from all other depths except 5 mm, and that 5 mm shows a significantly different with 9 mm. This indicates that indentation depths of 4 and 5 mm exhibit distinct perceptual characteristics compared to greater indentation depths (6 ~ 10 mm). For the indentation ratio, all levels showed significant differences except between 0.7 and 1.0.

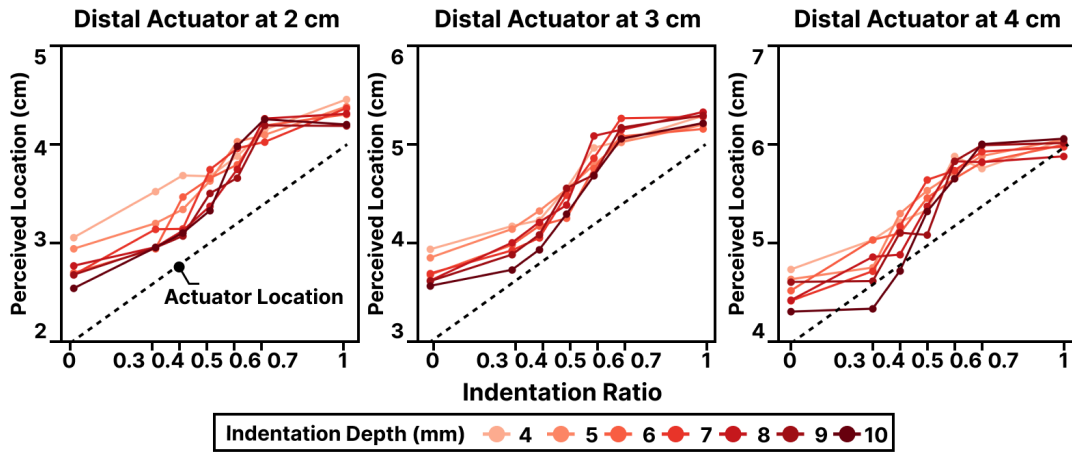


Fig. 4. Results of *Perception Study 2*. Users' perceived location by indentation ratio for different indentation depth levels and distal actuator location at (a) 2 cm, (b) 3 cm, and (c) 4 cm.

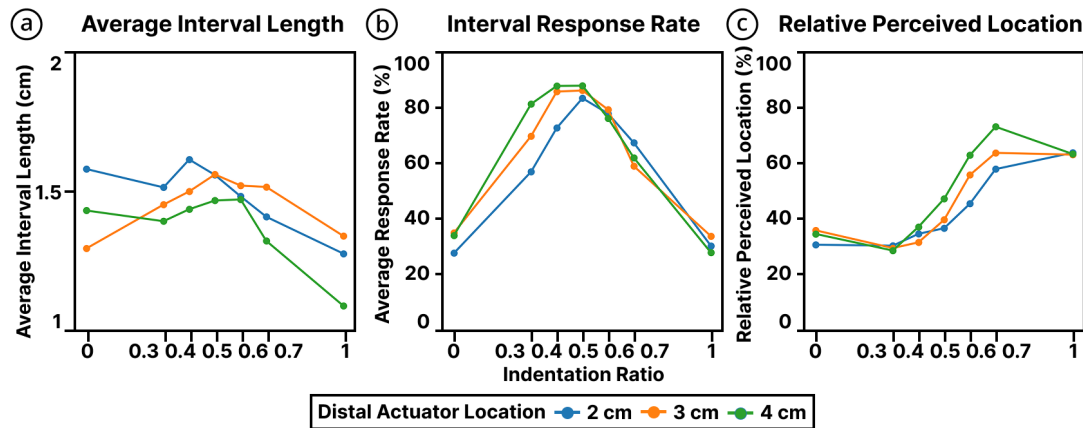


Fig. 5. Perception study 2 results. (a) Average length of the interval when users responded with an interval, (b) Response rate indicating how often users reported perceiving an interval, (c) Relative perceived location within the reported interval.

At the distal actuator position at 3 cm, a significant main effect was found for indentation depth ( $F(6, 102) = 2.4$ ,  $p < .024$ ) and indentation ratio ( $F(6, 102) = 102.7$ ,  $p < .001$ ). Post-hoc analyses revealed that the 4 mm and 10 mm indentation depths differed significantly. For the indentation ratio, all levels showed significant differences except between 0.3 and 0.4 and between 0.7 and 1.0. At the distal actuator position at 4 cm, a significant main effect was found for indentation ratio ( $F(6, 102) = 96.3.7$ ,  $p < .001$ ) but not for indentation depth ( $F(6, 102) = 1.75$ ,  $p = .107$ ). Post-hoc analyses for the indentation ratio showed significant differences except between 0.6 and 0.7 and between 0.7 and 1.0.

When participants responded the perceived location as intervals, the average length of the interval across all trials was 1.46 cm, whereas the actual physical distance between the two actuators was 3 cm (2 cm actuator spacing and 1 cm actuator diameter). For the distal actuator at 2 cm, the average length of the interval was 1.51 cm and 1.48 cm at 3 cm and 1.40 cm at 4 cm. Interval length did not differ significantly across conditions.

Table 3. Perceived location, interval start/end, and interval rates (mean value w/SD across indentation ratios and distal actuator positions of Perception Study 2. Perceived locations are shown in bold to highlight their modulation by the indentation ratio. Interval rate indicates the proportion of trials in which participants responded with an interval.

Indentation Ratio	Distal actuator at 2cm				Distal actuator at 3cm				Distal actuator at 4cm			
	Perceived Location (cm)	Interval Start (cm)	Interval End (cm)	Interval Rate (%)	Perceived Location (cm)	Interval Start (cm)	Interval End (cm)	Interval Rate (%)	Perceived Location (cm)	Interval Start (cm)	Interval End (cm)	Interval Rate (%)
0.0	<b>2.9 (0.9)</b>	2.4 (0.8)	3.9 (1.0)	28.0	<b>3.7 (0.7)</b>	3.3 (0.7)	4.6 (0.8)	35.0	<b>4.6 (0.9)</b>	4.1 (0.8)	5.5 (0.9)	34.0
0.3	<b>3.2 (0.9)</b>	2.7 (0.8)	4.2 (0.9)	57.0	<b>4.0 (1.0)</b>	3.6 (0.9)	5.0 (0.9)	70.0	<b>4.7 (1.2)</b>	4.4 (1.0)	5.7 (1.1)	81.0
0.4	<b>3.2 (1.1)</b>	2.7 (0.8)	4.3 (1.0)	73.0	<b>4.1 (0.9)</b>	3.7 (0.9)	5.2 (0.9)	86.0	<b>5.1 (1.1)</b>	4.5 (1.0)	6.0 (1.1)	88.0
0.5	<b>3.5 (1.1)</b>	2.9 (0.9)	4.5 (1.0)	83.0	<b>4.4 (1.1)</b>	3.8 (0.9)	5.3 (1.0)	86.0	<b>5.4 (1.2)</b>	4.7 (1.1)	6.1 (1.1)	88.0
0.6	<b>3.8 (1.1)</b>	3.1 (0.9)	4.6 (0.9)	78.0	<b>4.7 (1.1)</b>	3.9 (0.9)	5.4 (1.0)	79.0	<b>5.7 (1.1)</b>	4.8 (1.2)	6.3 (1.1)	76.0
0.7	<b>4.0 (1.1)</b>	3.2 (1.0)	4.6 (1.0)	67.0	<b>5.0 (1.0)</b>	4.1 (1.0)	5.6 (1.1)	59.0	<b>5.8 (1.0)</b>	4.8 (1.1)	6.2 (1.0)	62.0
1.0	<b>4.0 (0.9)</b>	3.2 (0.9)	4.5 (0.8)	31.0	<b>5.2 (0.9)</b>	4.3 (1.0)	5.7 (1.0)	34.0	<b>6.0 (0.7)</b>	5.2 (1.0)	6.3 (0.8)	28.0

The proportion of trials in which participants responded with an interval was highest when the indentation ratio was 0.5, and lowest at 0 and 1 in Figure 5b. For the distal actuator at 2 cm, the proportion of responses across the seven indentation ratios (0 to 1.0) was 28.1%, 57.0%, 72.6%, 83.2%, 77.7%, 67.3%, 30.7% showing a rise and fall pattern peaking at a 0.5 ratio. For the distal actuator at 3 cm the proportion was 35.3%, 69.7%, 85.5%, 85.9%, 79.1%, 59.0%, 34.1%. For the distal actuator at 4 cm the proportion was 34.4%, 81.1%, 87.6%, 87.6%, 76.0%, 62.0%, 28.3%.

In addition, when participants responded with an interval, the location of the maximum perceived point is shown in Figure 5c. As the indentation ratio increased, the relative perceived location also shifted toward the proximal side. This trend is reasonable because a higher perceived location indicates stronger stimulation near the proximal actuator, which aligns with the fact that increasing the indentation ratio results in a greater indentation depth at the proximal actuator. At the 2 cm distal actuator location, the relative perceived location gradually increased across the indentation ratios (0 to 1.0), with values of 31.1%, 30.8%, 35.0%, 37.0%, 45.7%, 58.0%, and 63.8%. At 3 cm, the relative perceived locations were 36.2, 29.9%, 31.9%, 40.0%, 55.9%, 63.8%, and 63.1%, and at 4 cm, the relative perceived locations were 34.9%, 29.0%, 37.4%, 47.5%, 62.9%, 73.1%, and 63.4%.

Finally, similar to Perception Study 1, we found the proximal bias with an average value of 0.47 cm across all trials. For the distal actuator at 2 cm, the proximal bias was 0.58 cm and 0.49 cm for the distal actuator at 3 cm and 0.34 cm for the distal actuator at 4 cm.

**4.3.3 Discussion.** In this study, we found that user-perceived locations varied by indentation ratio and indentation depth. This suggests that a moving phantom sensation can be achieved, as the perceived location of the stimulus shifts progressively with an increasing indentation depth at either the proximal or distal actuator. While this is an intuitively expected result, such a tendency has not been thoroughly examined in the context of pressure-based phantom sensation. This study reaffirms the presence of this phantom sensation trend through empirical validation. Furthermore, we also observed a proximal bias in this study. Similar to Perception Study 1, the current results demonstrate that a proximal bias emerges even during phantom sensation during the modulation of two actuators' indentation depth. The underlying causes of proximal bias and potential strategies for accounting for it in haptic rendering scenarios are addressed in more detail in the Discussion.

We also observed an intriguing finding that the perceived location varied depending on the indentation depth. As the indentation depth increased, users tended to perceive the pressure sensation further in the distal direction, indicating a reduction in proximal bias. This aligns with previous findings [34, 47] that greater skin deformation enhances tactile sensitivity. In other words, stronger stimuli enable users to localize pressure sensations more accurately. Additionally, the experimental results show that 4 mm and 5 mm indentation depths were significantly different from the deeper indentation depths (6, 7, 8, 9, 10mm). Therefore, depths up to 5 mm were classified as

Table 4. Results of *Perception Study 3*. Average measured threshold and normalized threshold for each condition. Normalized threshold = measured threshold / indentation depth.

Indentation Depth	Distal actuator at 2 cm		Distal actuator at 3 cm		Distal actuator at 4 cm	
	Measured threshold (mm)	Normalized threshold	Measured threshold (mm)	Normalized threshold	Measured threshold (mm)	Normalized threshold
5 mm	3.8	0.76	3.4	0.69	3.9	0.77
8 mm	6.5	0.81	6.4	0.80	6.0	0.75

producing weak pressure sensations in the USH, while greater depths were categorized as strong pressure. In subsequent experiments, indentation depths were selected from each group accordingly.

#### 4.4 Perception Study 3: Midpoint Stimulus vs Phantom Sensation

**4.4.1 Methods.** The naive approach to implementing a moving phantom sensation is to linearly modulate the amplitude of two actuators over time. However, in the context of vibrotactile feedback, this linear profile reveals an attenuated sensory response at the midpoint in vibrotactile feedback [2]. To investigate whether a similar attenuation occurs with pressure-based phantom sensation, we designed an experiment to quantitatively assess the extent of the diminished pressure sensation at the midpoint. Specifically, this study aims to determine the indentation depth required from each actuator to match the perceived intensity of a single midpoint stimulus with an indentation of  $h$  mm. We adopted the simple up-and-down method [15, 26, 35] and employed the same device used in the previous study.

**Study Setup** We recruited 18 participants (8 female,  $23.5 \pm 3.52$  years old) for the experiment. Participants filled out written informed consent before the experiment. To investigate the effects of indentation depth, we set two different indentation depths for a single midpoint stimulus, 5 mm, and 8 mm based on the classification in *Perception Study 2* as low and high indentation depth conditions, respectively. We also set three different distal actuator locations: 2 cm, 3 cm, and 4 cm. The proximal actuator is located 2 cm away relative to the distal actuator. Each distal actuator location was blocked, and all other experimental conditions were randomized within blocks. Block order was systematically balanced across participants using a Latin Square. Thus, each participant was tested with a total of 6 conditions (2 indentation depths  $\times$  3 distal actuator locations).

**Procedure** A two-interval one-up one-down double staircase procedure was used. On each trial, the participant was presented with two consecutive stimuli, and a 2AFC (Two-alternative forced choice) method was used to choose the stronger stimulus. The order of a single midpoint stimulus and two-point stimuli, and the order of the ascending and descending are randomized. In the ascending order condition, since the intensity of the phantom sensation needs to be lower compared to the single midpoint stimulus, we activated each actuator by 0.5 mm for the 5 mm condition, and 3 mm for the 8 mm condition. For the descending order, to ensure the stronger sensation for phantom sensation, the initial indentation depth was 5 mm for the 5 mm condition and 10 mm for the 8 mm condition. We determined these parameters through a pilot study, selecting sufficiently strong or weaker sensations. We set the 6 reversals, and we calculated the threshold with the last 4 reversals. We set the step size at 2 mm until the first reversal, and we reduced it to 1 mm until the third reversal, and after we fixed it at 0.5 mm. A 2 mm step size means that each actuator indentation depth is decreased by 1 mm.

Participants received a brief study overview and calibration before starting the main session. In each trial, participants performed a 2AFC identifying the more intense stimulus, and the condition ended upon reaching six reversals. Between each condition, participants rested for about a minute and continued with the following condition with an additional calibration process.

**4.4.2 Results.** Table 4 presents the results in this study. The measured threshold of 3.8 mm for 5 mm indentation depth and a distal actuator location of 2 cm indicates that to replicate a 5 mm single midpoint stimulus at 2 cm

on USH, each of the two actuators should be indented by  $3.8\text{ mm}$ . We assumed that this result is proportional to the indentation depth; thus, we divided the threshold by the indentation depth level to get a normalized threshold (Figure 6a). Normalized threshold appears consistent across all conditions. For statistical analysis, we conducted a two-way repeated-measure ANOVA with two factors: indentation depth and distal actuator location. The analysis revealed no significant effect for either factor, indentation depth:  $F(1, 17) = 3.23, p = .09$  and distal actuator location:  $F(2, 34) = 0.87, p = .43$ . The overall average of the normalized threshold was 0.76. This result indicates that to deliver equal intensity of a  $y\text{ mm}$  pressure sensation at the  $x\text{ cm}$  location, the two actuators located at  $x - 1\text{ cm}$  and  $x + 1\text{ cm}$  should each indent to  $0.76 \times y$ .

**4.4.3 Discussion.** In this experiment, we analyzed the needed indentation depth for two actuators inducing phantom sensations to replicate the single midpoint stimulus. The results show that both actuators must be driven to an indentation depth of stimulus multiplied by 0.76 to replicate the midpoint sensation. This result is quite notable in that we obtained consistent results regardless of the indentation depth or the specific location of the actuators.

The ratio of 0.76 indicates that inducing pressure-based phantom sensation through two actuators requires a stronger actuation than simply driving each actuator at 0.5 intensity, as in a linear amplitude modulation. This observation aligns with previous findings in vibrotactile feedback [2], where linear amplitude modulation tends to produce a weakened sensation near the midpoint. Therefore, we can expect that users prefer a profile that delivers greater intensity at the midpoint than a simple linear modulation as in vibrotactile feedback [50].

## 5 RACK-AND-PINION-DRIVEN WEARABLE HAPTIC DEVICES

Building on the results from previous perception studies, we aimed to implement a wearable haptic device capable of rendering pressure-based moving phantom sensations. We designed the haptic device based on the following design rationale. First, the device needed to precisely modulate the indentation depth while ensuring non-backdrivability, allowing it to resist deformation caused by external force. Second, the total device weight had to remain below 100 g to ensure wearability.

To satisfy the first design rationale, the device needed a mechanism capable of precisely rendering the target indentation depth while exhibiting non-backdrivability to resist deformation under external loads. Thus, we

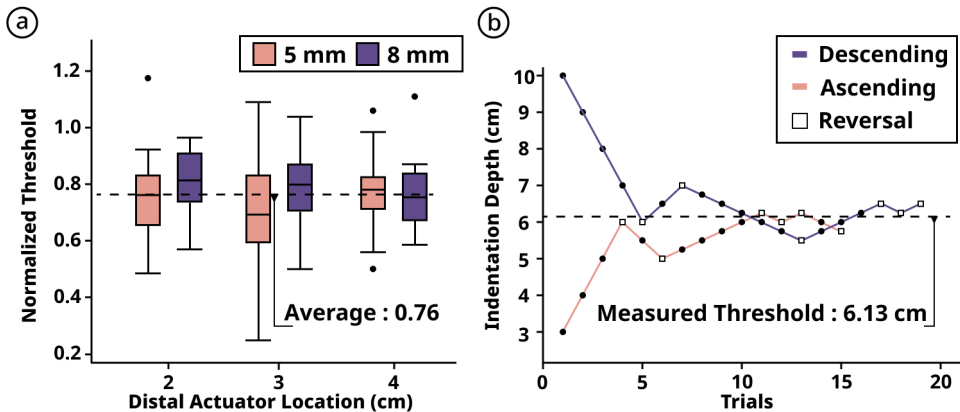


Fig. 6. Results of Perception Study 3 (a) The graph illustrates the normalized threshold by different distal actuator locations and indentation depth levels. There were no significant differences across conditions. (b) Result from P3, with an 8 mm indentation depth, and the distal actuator located at 3 cm.

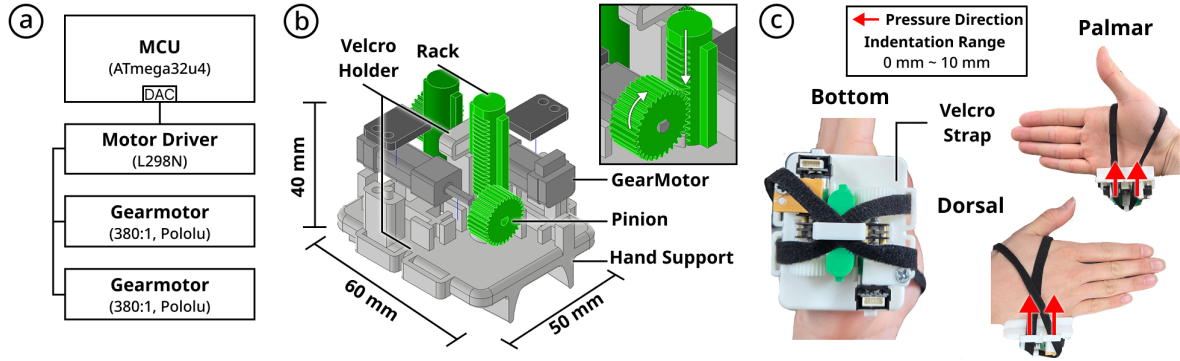


Fig. 7. Our rack-and-pinion-driven wearable haptic device. We control the pinion rotations to render the target indentation depth. Our hardware (a) configurations and (b) structures. (c) Bottom, palmar, and dorsal views.

determined a motor-based actuation system, which allows precise control through the integration of additional sensors. Specifically, we implemented a motor-driven rack-and-pinion mechanism, using a motor encoder to regulate the pinion's rotation and, consequently, the indentation depth. To achieve non-backdrivability, we employed a high-gear-ratio motor.

The rack-and-pinion structure also satisfies the second design rationale. Traditional motor-driven linear motion systems often employ lead screw mechanisms. However, a major drawback of lead screws is that they extend the device vertically from the contact surface, increasing the device's height [31]. In the Pocopo [69] system, a worm gear was employed to reorient the lead screw laterally, but this modification increased the device's lateral footprint. To address these limitations, we adopted a rack-and-pinion mechanism that converts motor rotation into linear motion while maintaining a compact form factor suitable for wearable applications. Our final device weighs only 50 g, which is significantly lighter than a typical smartphone (about 200 g), making it highly wearable.

Figure 7 illustrates the design of our wearable devices. We fabricated the rack-and-pinion structure using a 3D printer. Additionally, we designed a custom 3D-printed frame for a velcro holder and hand support (Figure 7b). To accommodate various hand sizes, we secured the device with adjustable velcro straps. We carefully designed the strap placement to align with the device's center of mass, minimizing unwanted movement during operation (Figure 7c). The straps also ensured consistent contact between the USH and the actuator's contact point. The device uses two servomotors (380:1 servomotor with 12 CPR encoders, Pololu) controlled by an L298N motor driver. Each motor has a no-load speed of 85 RPM, and a stall torque of 5.0 kg · cm. The pitch circle's diameter of the pinion is 16 mm, resulting in a maximum rack speed of approximately 50 mm/s. The overall height of the device is approximately 40 mm.

We used an Arduino Leonardo (ATmega32u4) to operate the wearable device. The Leonardo communicates with the PC via serial communication and sends digital signals to the motor driver to operate the motors. Once we set the target indentation depth, the system calculates the corresponding number of pinion rotations and drives the motor until the encoder value reaches the desired count. This closed-loop control enables the system to render the specified indentation depth accurately, thereby providing precise pressure feedback.

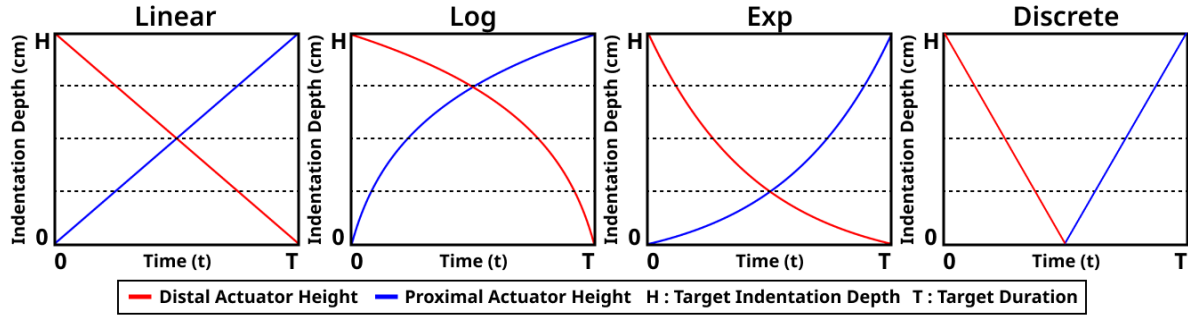


Fig. 8. Indentation depth profiles of two actuators during rightward pressure rendering. We compared four different rendering methods *Linear*, *Log*, *Exp*, *Discrete* to identify the most natural approach for conveying pressure movement. *Discrete* is the naive approach without phantom sensation.

## 6 USER STUDY

### 6.1 Rendering Method Evaluation

Finally, we aimed to identify an appropriate rendering profile of pressure-based moving phantom sensation for natural pressure movement sensation. To this end, we compared several rendering profiles. Based on the findings from [Perception Study 3](#), which indicated that users perceived a stronger indentation depth from two actuators as equivalent to a single midpoint stimulus, we hypothesized that the logarithmic profile, which renders a stronger sensation at the midpoint, would be preferred. This expectation aligns with prior preferences for vibrotactile phantom sensation [2, 51].

**Study Setup** We recruited 18 participants (10 female,  $25.7 \pm 3.8$  years old) for this experiment. All participants provided written informed consent before participation. Participants were paid \$10 for their participation in an IRB-approved study. In this experiment, we employed a four-factor within-subject factorial design to validate the appropriate rendering profile for pressure-based moving phantom sensations, using an experimental setup similar to that of prior vibrotactile research [29]. Since no established rendering method exists for pressure-based moving phantom sensation, we defined four distinct rendering profiles, including one commonly used in previous phantom sensation studies, and conducted comparative experiments.

The first condition is a linear condition (*Linear*), in which the heights of the two actuators vary linearly over time. The second condition is a logarithmic condition (*Log*), where the actuator trajectories are defined by Eq. 1 and Eq. 2, with  $H$  denoting the target indentation depth,  $T$  representing the target duration,  $P$  and  $D$  denoting the proximal and distal actuator. We adopted a logarithmic equation to generate a stronger stimulation near the midpoint and to produce an indentation depth curve resembling a logarithmic function, rather than to precisely model a mathematical equation. The shape of the *Log* equation resembles the logarithmic profile used in vibrotactile phantom sensation. We set the parameter  $\alpha$  to 10.44 so that the actuator output at the midpoint reaches three-quarters of the target indentation depth. The third condition is the exponential condition (*Exp*), defined by Eq. 3 and Eq. 4. We set the parameter  $\beta$  to 2.2 to ensure that the actuator output at the midpoint reaches one-quarter of the target indentation depth. Likewise, we focus on designing the profile to render a weak sensation at the midpoint. The final condition, the *Discrete* condition, serves as a baseline without inducing phantom sensation. In this case, the two actuators operate independently based on the stimulus location. Figure 8 shows detailed graphs of each rendering profile.

$$H_P = H \times \frac{\ln(1 + \alpha \times \frac{t}{T})}{\ln(1 + \alpha)} \quad (1)$$

$$H_D = H \times \frac{\ln(1 + \alpha(1 - \frac{t}{T}))}{\ln(1 + \alpha)} \quad (2)$$

$$H_P = H \times \frac{e^{\beta \times \frac{t}{T}} - 1}{e^\beta - 1} \quad (3)$$

$$H_D = H \times \frac{e^{\beta \times (1 - \frac{t}{T})} - 1}{e^\beta - 1} \quad (4)$$

The user study included four independent variables: **Profile** (*Log, Linear, Exp, Discrete*), **Indentation Depth** (5 mm and 8 mm), **Duration** (2.0s and 4.0s), and **Direction** (left and right). We selected the value of **Duration** to allow users sufficient time to perceive the pressure-based moving phantom sensations and also considered prior research indicating that handshakes last over 3 s [40]. For the **Direction**, left indicates movement from the proximal to the distal on USH, and right refers to the opposite direction. We completely randomized **Profile**, **Indentation Depth**, **Duration**, while **Direction** was counter-balanced. Each participant completed all 32 experimental conditions (4 **Profile**  $\times$  2 **Indentation Depth**  $\times$  2 **Duration**  $\times$  2 **Direction**), repeated over four blocks, resulting in a total of 128 trials per participant. For analysis, we used only data from the final three blocks. All conditions were randomized within each block.

When delivering pressure feedback via the rack-and-pinion mechanism, we first actuated the device to position the actuators at their starting points and reset the actuators after each stimulus. During both initialization and resetting, the actuators moved at a constant speed of 10 mm/s. After initialization, the device remains stationary for 2 seconds before delivering the pressure-based moving phantom sensation. We asked participants to evaluate only this moving phantom sensation. To avoid applying direct pressure to MCP joints, we positioned the distal actuator at a 3 cm location, consistent with the layout used in the perception study.

To induce a more natural sensation of pressure movement, we evaluated the user's subjective perceptions of the continuity and consistency of the rendered sensation. Maintaining *continuity*, particularly at the midpoint of the stimulation path, is essential for evoking the illusion of smooth pressure movement. Moreover, sustaining *Consistency* in intensity provides the design guideline for rendering both stronger and weaker pressure movements. Based on these considerations, we selected these two perceptual dimensions as evaluation criteria. Participants rated *Continuity* and *Consistency* on a scale ranging from 0 to 100. These metrics have also been used in prior studies investigating vibrotactile moving phantom sensation [8].

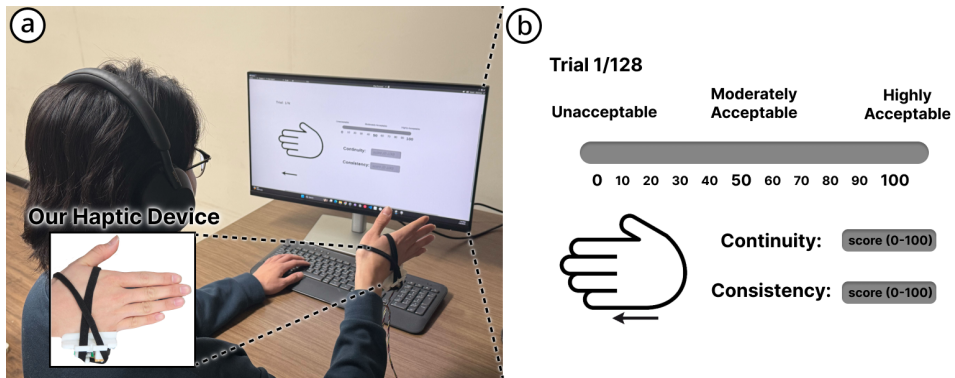


Fig. 9. User study setup. (a) A participant wearing the haptic device on the right hand. (b) GUI used for rating the *continuity* and *consistency* of each stimulus on a 0-100 scale.

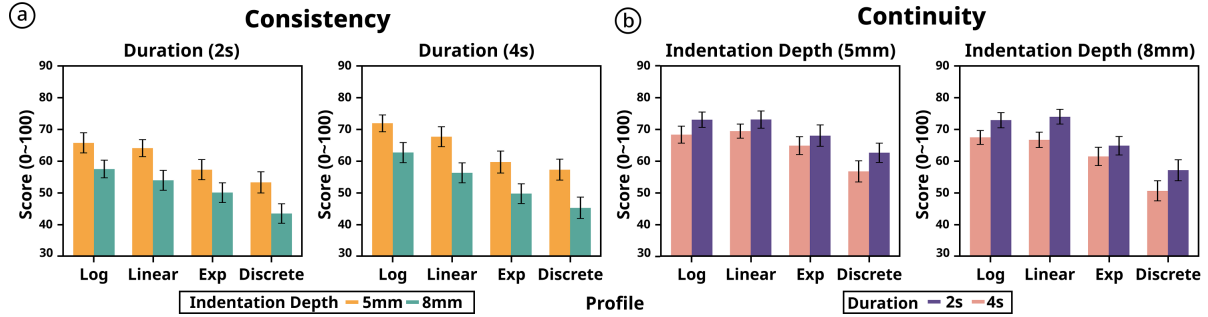


Fig. 10. Mean score for (a) *Consistency* and (b) *Continuity* for four rendering profiles (*Log*, *Linear*, *Exp*, *Discrete*).

Table 5. Scores (mean value w/SD) for *consistency* and *continuity* under each experimental condition. Overall, the *Log* profile yielded the highest consistency score, while the *Linear* profile yielded the highest *continuity* score in most cases.

Metric	Profile	Duration		Indentation Depth		Direction	
		2 s	4 s	5 mm	8 mm	Left	Right
Consistency	<i>Log</i>	<b>61.6 (18.1)</b>	<b>67.2 (17.8)</b>	<b>68.7 (17.5)</b>	<b>60.1 (17.8)</b>	<b>61.4 (19.0)</b>	<b>67.4 (16.8)</b>
	<i>Linear</i>	59.0 (18.0)	61.9 (19.4)	65.8 (17.3)	55.1 (18.6)	57.2 (19.5)	63.7 (17.3)
	<i>Exp</i>	53.7 (19.0)	54.7 (20.1)	58.5 (19.7)	50.0 (18.4)	52.1 (18.4)	56.3 (20.4)
	<i>Discrete</i>	48.4 (19.6)	51.3 (20.7)	55.3 (19.7)	44.5 (19.2)	47.6 (19.4)	52.2 (20.7)
Continuity	<i>Log</i>	67.8 (14.5)	72.8 (14.2)	70.6 (15.3)	70.1 (13.8)	70.5 (14.5)	<b>70.2 (14.7)</b>
	<i>Linear</i>	<b>68.0 (13.7)</b>	<b>73.4 (14.9)</b>	<b>71.2 (14.7)</b>	<b>70.2 (14.4)</b>	<b>71.7 (12.3)</b>	69.7 (16.5)
	<i>Exp</i>	63.1 (16.8)	66.4 (18.7)	66.4 (18.3)	63.1 (17.3)	67.3 (15.3)	62.1 (19.8)
	<i>Discrete</i>	53.7 (19.5)	59.8 (18.9)	59.7 (19.0)	53.9 (19.5)	55.8 (19.1)	57.8 (19.8)

**Procedure** After a brief explanation of the experimental protocol, participants wore the wearable device (Figure 9a) on their right hand. Participants initiated each trial by pressing the spacebar to trigger the stimulus. Using the graphical user interface (GUI) shown in Figure 9b, participants rated the *Continuity* and *Consistency* of each stimulus and then pressed the spacebar again to proceed to the next trial. After completing the main session, participants were briefly interviewed about their pressure experience. Breaks were allowed between trials, and the entire session lasted approximately one hour.

## 6.2 Results

We conducted four-way repeated measures ANOVA for each of the two perceptual measures: *Consistency* and *Continuity*. In Table 5, the highest-scoring profile for each condition is highlighted in bold. The following section reports the detailed statistical results for both metrics.

**Consistency** The four-way repeated measures ANOVA revealed a significant main effects for all factors: **Profile**;  $F(3, 51) = 47.01, p < .001$ , **Indentation Depth**;  $F(1, 17) = 38.69, p < .001$ , **Duration**;  $F(1, 17) = 6.37, p = .022$ , and **Direction**;  $F(1, 17) = 5.146, p = .037$ . In addition, significant interaction effects emerged between **Indentation Depth × Direction**;  $F(1, 17) = 7.48, p = .014$  and **Profile × Direction × Duration**;  $F(3, 17) =$

$5.44, p = .032$  was significant. Figure 10a visualizes the average score across **Profile** and **Indentation Depth**. User ratings tended to decline toward the *Discrete*, while lower **Indentation Depth** received more favorable ratings. To clarify these preferences, we divided the data by **Duration** to entangle these interaction effects. If **Duration** was 2 second, **Profile**;  $F(3, 51) = 21.8, p < .001$  were significant. Tukey's HSD test reveals that *Linear* and *Log* significantly get higher scores than *Discrete*. If **Duration** was 4 second, **Profile**;  $F(3, 51) = 23.9, p < .001$  and **Direction**;  $F(1, 17) = 6.7, p = 0.019$  were significant. Post-hoc analysis reveals that *Linear* and *Log* get higher scores than *Discrete* and *Log* get higher scores than *Exp*.

**Continuity** The four-way repeated measures ANOVA revealed significant main effects for **Profile**;  $F(3, 51) = 23.35, p < .001$  and **Duration**;  $F(1, 17) = 7.01, p = .017$ . Additionally, significant interaction effects were found between **Indentation Depth**  $\times$  **Profile**;  $F(3, 51) = 10.41, p = .005$ , and **Duration**  $\times$  **Direction**  $\times$  **Profile**;  $F(3, 17) = 8.15, p = .011$ . To clarify these preferences, we divided the data by **Duration** to entangle these interaction effects. If **Duration** was 2 second, **Profile**;  $F(3, 51) = 20.9, p < .001$  were significant. We conducted Tukey's HSD test for the **Profile** and found that *Exp*, *Linear*, and *Log* get significantly higher scores than *Discrete*. If **Duration** was 4 second, **Profile**;  $F(3, 51) = 13.2, p < .001$  and the interaction between **Profile** and **Duration**;  $F(3, 51) = 4.3, p = .008$  was significant. *Log* were significantly higher than *Discrete* and *Exp* but there was no significant difference between *Linear* and *Log*.

**User Feedback** We gathered user feedback on their experiences with the pressure-based moving phantom sensation during the study. Several participants (*P11, P12*) noted the differences across profiles were more apparent in terms of *Consistency* than *Continuity*. This indicates that achieving *Consistency* is harder than *Continuity*. Regarding *Consistency*, many participants (*P2, P3, P11, P14, P17*) reported that the stimulus intensity tended to weaken at the midpoint. Notably, *P2* described the sensation of intensity forming a V-shaped profile, with the midpoint feeling distinctly weaker than the edge. Additionally, participants (*P8, P12, P17*) indicated that the stimulus felt more continuous when its intensity was lower. When the stimulus was strong, users more easily detected intensity fluctuations in *Continuity* and *Consistency*.

### 6.3 Discussion

By comparing four rendering methods, we identified the most effective profile for delivering natural pressure movement feedback across various conditions. For *Consistency*, the *Log* profile consistently received the highest ratings across all conditions, aligning with the assumption from the result *Perception Study 3*. For *Continuity*, both the *Log* and *Linear* profiles achieved the top scores. These results replicate trends observed in prior vibrotactile studies [2, 50] that users prefer a logarithmic profile over a linear profile. Therefore, to achieve a realistic pressure-based moving phantom sensation, a *Log* profile is recommended for enhancing both *Consistency* and *Continuity*. The overall average score for *Log* and *Linear* was 60.5 and 64.4 for *Consistency* and 70.7 and 70.3 for *Continuity*. As shown in Figure 9b, we represent the GUI, which shows the direction and the pressure movement. We infer that the higher scores given to the *Log* and *Linear* profiles, compared to other profiles, reflect users' perception of more realistic pressure movement and direction. In fact, most users reported that the sensation of moving pressure was clearly perceived under certain conditions. These findings suggest that the system successfully evoked a pressure-based moving phantom sensation with a wearable form factor. However, the current study did not verify whether the sensation can be elicited while the user's hand is in dynamic motion or interacting with other objects. Future studies will investigate whether the moving phantom sensation can still be reliably evoked under various hand conditions.

In addition to the factor **Profile**, **Duration** also played a significant role. Longer stimulus durations resulted in higher user ratings, likely because gradual changes in indentation depth were perceived as more stable and comfortable. Regarding the **Indentation Depth**, the lower indentation depth (5 mm) tended to receive higher scores for both *Consistency* and *Continuity*. Several participants reported that higher indentation depth negatively

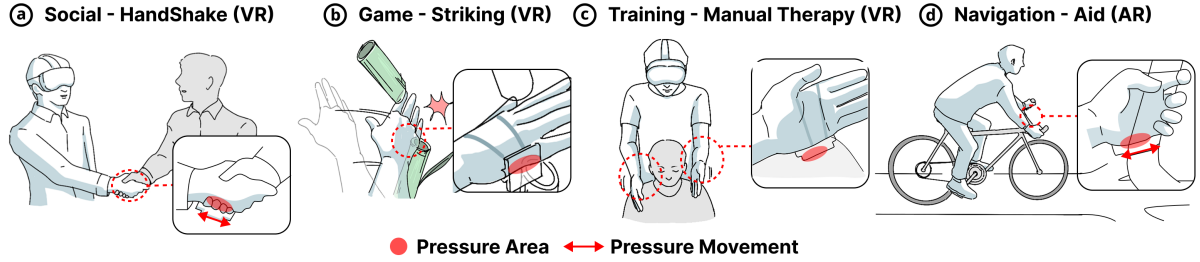


Fig. 11. Moving-Press renders natural pressure movement feedback for (a) rendering a tactile handshake during a virtual meeting to enhance social presence, (b) conveying striking sensations in a game interaction scenario, (c) delivering pressure stimulus during manual therapy training, (d) providing directional cues through spatial pressure shifts during navigation tasks.

influenced their ratings, with *P1* noting that a loss of *Consistency* became more noticeable under high indentation depth conditions. The factor **Direction** also had a significant effect on *Consistency*. Users preferred stimuli that moved from distal to proximal. This preference may reflect the tendency to favor stimuli that terminate in the proximal area, which has thicker, softer skin, rather than in the distal region near the firmer MCP joint.

## 7 APPLICATION

Moving-Press renders pressure movement feedback on the USH. By employing a rack-and-pinion mechanism, the device delivers pressure feedback in a compact and wearable form factor. To evoke pressure-based moving phantom sensation, users need to carefully design the actuator spacing and fasten it correctly to measure the correct contact point between the actuators and the skin. Once the device is properly positioned on the user, the sensation of movement can be most realistically reproduced by applying logarithmic driving profiles of two actuators. In addition to rendering continuous movement, static phantom sensations can also be induced between the actuators depending on their indentation depth configuration. In the following section, we present a potential application scenario that leverages the design and empirical findings of this study. In the future, we plan to experimentally validate whether users can perceive the pressure movement naturally while wearing the device and moving freely in VR, thereby demonstrating its practical applicability.

In VR environments, users can communicate with others regardless of physical distance. During social interactions such as virtual meetings and negotiations, communication extends beyond verbal exchanges to include tactile gestures, most notably, handshakes. Handshake is a meaningful emotional interaction between two people [5, 41, 59]. Moving-Press realistically render pressure variations on the USH region caused by the contact from the partner's index to pinky during a handshake. Compared to uniformly applying pressure across the entire area, this approach enables a more realistic reproduction of tactile sensations. Moving-Press can also support various game scenarios. When the user's hand transforms into a sword, it can render impact sensations upon striking a target, as well as simulate pressure movement during sliding motion. It can also replicate the karate chop, providing realistic feedback in martial arts contexts. Next, Moving-Press can be utilized as an assistive tool in manual therapy training. Finally, pressure movement can further be utilized to provide intuitive haptic cues for navigation, such as guiding users along a path in outdoor scenarios (Figure 11).

## 8 DISCUSSION

In this study, we conducted an in-depth investigation of the pressure-based moving phantom sensation for rendering natural pressure movement. Beyond establishing perceptual findings, we developed a wearable device

and introduced the haptic interface, Moving-Press, demonstrating its applicability across various VR scenarios. We found that pressure-based phantom sensation can be reliably elicited on the ulnar-sided hand using two actuators spaced 2 cm apart. Furthermore, users preferred a logarithmic profile for pressure-based moving phantom sensation. We also observed the perceptual characteristics that users' perceived location is proximally biased, and this bias decreases as the indentation depth increases. Finally, there was a linear relationship between the perceived intensity of the one-point stimulus and the perceived intensity of the phantom sensation.

### 8.1 Mechanism of Pressure-based Phantom Sensation

When a stimulus is applied to the skin, its perceived intensity is strongest near the point of contact and gradually diminishes with distance [63]. Therefore, when the strong sensation regions of two stimuli overlap, they are perceived as a single unified sensation. However, when the distance from the stimulus exceeds a certain threshold, an area of inhibition emerges, which reduces the perceived intensity in that area. As a result, two stimuli are perceived separately rather than merging. Thus, it is essential to consider this distance threshold when designing for phantom sensation. On the USH, this threshold for perceptual enhancement is approximately 2 cm. This result shows that pressure-based phantom sensations emerge on the hand, and that vibration is not the only viable method for evoking the moving phantom sensation.

### 8.2 Proximal Bias and Indentation Depth Effect

An interesting and consistent observation during the study was that users tended to perceive stimuli applied to the USH as being shifted in the proximal direction. In *Perception Study 1*, the proximal bias was 0.76 cm for one-point stimulus and 0.59 cm for two-point stimuli, and 0.47 cm in *Perception Study 2*. A consistent proximal bias of approximately 0.6 cm was observed. In this section, we discuss potential causes of this bias and propose strategies to compensate for it in practical rendering environments.

One potential explanation for this perceptual bias is due to the anchor effect. Users often localize tactile stimuli toward salient anatomical landmarks, which has been observed on other body regions [27]. In this study, we speculate that the wrist served as an anchor, contributing to the observed proximal bias.

A second explanation is from the variations in skin fleshiness within the USH region. Previous study [44] has shown that different areas of the hand vary in skin stiffness and deformability. The degree of fleshiness varies across different regions of the hand, and even within the targeted USH area, the skin tends to become softer from distal to proximal. Prior research [36] showed that humans with softer skin could better discriminate the stimulus. Therefore, the softer area may have been more sensitive along the ulnar border and led users to perceive the given stimulus as being located more proximally.

To implement the pressure-based moving phantom sensation on practical VR scenarios, both the proximal bias and the influence of indentation depth in reducing it should be taken into account. The device needs to be positioned slightly distal (about 0.6 cm) to the target area to precisely target the location. Moreover, the required offset should be adjusted according to the indentation depth, as the proximal bias decreases with greater depth. This allows haptic designers to deliver pressure sensations more accurately to the intended target area.

### 8.3 Limitation and Future Work

While our research offers valuable insights into the pressure-based moving phantom sensation, our study also presents certain limitations. In this section, we summarize the key findings and limitations of our approach.

During this study, we observed pressure-based phantom sensation and moving phantom sensation. The USH region selected in our experiment has clear potential for use in scenarios such as handshakes, and we plan to validate in future user studies whether the device enhances immersion in such interactions. However, we note that this region represents a relatively specialized area. However, it is encouraging that previous work [63] has

reported that two pressure stimuli applied to the MCP joint area of the palm are perceived as a single unified sensation, suggesting potential for extension to other regions of the palm. Also, the pressure funneling effect has been validated in the forearm [17], which implies the potential for applying moving phantom sensation to other body parts. Therefore, pressure-based moving phantom sensation shows promise for application to other body parts, and we plan to conduct studies to determine the specific method for practical rendering scenarios.

A second limitation is that the experiment was conducted with a fixed actuator diameter of 1 cm and found a relatively small 2 cm threshold for phantom sensation. The facts that actuator size influences perceived sensation [57], and that a 2 cm spacing limits device miniaturization, underscore the need for further research into various actuator sizes and layouts. Previous studies have reported that tactile summation can occur even with actuator tips as small as 2 mm in diameter [63], suggesting that moving phantom sensations may be achievable with a wide range of actuator sizes. In addition to actuator size, the relatively small 2 cm spacing also provides mechanical advantages. Because it does not require physical movement, the system maintains high mechanical stability, and the absence of hardware in the central region of the two actuators contributes to a more lightweight and compact form factor. This design becomes even more beneficial on body regions with larger summation thresholds. For example, spatial summation has been reported to occur across distances of up to 6.1 cm on the forearm [17]. Building on this finding, future studies may investigate whether moving phantom sensations can be effectively rendered along the full length of the forearm using a sparse actuator array by modulating pressure intensity across spatially distributed actuators.

While users preferred the logarithmic profile for rendering pressure-based moving phantom sensations, a precise mathematical formulation has yet to be established. In vibrotactile feedback, researchers have developed rendering methods based on the energy summation model in the Pacinian channels [19, 38] and others have proposed techniques for delivering feedback along curved paths [43]. In the case of pressure feedback, more refined models could be developed by incorporating the physical properties of the skin [39, 53].

## 9 CONCLUSION

During VR interactions such as grasping, pressing, or manipulating objects, users feel pressure movement across the hand. To render realistic pressure movement, we integrated the pressure-based phantom sensation into a rack-and-pinion-driven wearable haptic device. We first validated that the maximum spacing of 2 cm between two actuators reliably induces pressure-based phantom sensation on the ulnar-sided hand. Based on these findings, we designed the wearable device and propose a Moving-Press to render pressure movement in a compact form factor. Our user study revealed that a logarithmic rendering profile produced a more natural sensation of pressure movement compared to other profiles. We believe that the findings of this study broaden the design space for rendering pressure movement, contributing to more immersive and engaging VR experiences.

## Acknowledgments

This work was partly supported by Electronics and Telecommunications Research Institute(ETRI) grant funded by the Korean government (25ZC1200, 50%) and the National Research Council of Science & Technology (NST) grant by the Korea government (MSIT) (No. CRC21014, 50%).

## References

- [1] Marco Aggravi, Florent Pausé, Paolo Robuffo Giordano, and Claudio Pacchierotti. 2018. Design and evaluation of a wearable haptic device for skin stretch, pressure, and vibrotactile stimuli. *IEEE Robotics and Automation Letters* 3, 3 (2018), 2166–2173.
- [2] David S Alles. 1970. Information transmission by phantom sensations. *IEEE transactions on man-machine systems* 11, 1 (1970), 85–91.
- [3] Betsy App, Daniel N McIntosh, Catherine L Reed, and Matthew J Hertenstein. 2011. Nonverbal channel use in communication of emotion: how may depend on why. *Emotion* 11, 3 (2011), 603.

- [4] Hrvoje Benko, Christian Holz, Mike Sinclair, and Eyal Ofek. 2016. Normaltouch and texturetouch: High-fidelity 3d haptic shape rendering on handheld virtual reality controllers. In *Proceedings of the 29th annual symposium on user interface software and technology*. 717–728.
- [5] Timothy W Bickmore, Rukmal Fernando, Lazlo Ring, and Daniel Schulman. 2010. Empathic touch by relational agents. *IEEE Transactions on Affective Computing* 1, 1 (2010), 60–71.
- [6] Elodie Bouzbib, Marc Teyssier, Thomas Howard, Claudio Pacchierotti, and Anatole Lécuyer. 2023. Palmex: Adding palmar force-feedback for 3d manipulation with haptic exoskeleton gloves. *IEEE Transactions on Visualization and Computer Graphics* (2023).
- [7] Harold E Burtt. 1917. Tactual illusions of movement. *Journal of experimental Psychology* 2, 5 (1917), 371.
- [8] Jongeun Cha, Lara Rahal, and Abdulmotaleb El Saddik. 2008. A pilot study on simulating continuous sensation with two vibrating motors. In *2008 IEEE International Workshop on Haptic Audio visual Environments and Games*. IEEE, 143–147.
- [9] William F Chaplin, Jeffrey B Phillips, Jonathan D Brown, Nancy R Clanton, and Jennifer L Stein. 2000. Handshaking, gender, personality, and first impressions. *Journal of personality and social psychology* 79, 1 (2000), 110.
- [10] Roger W Cholewiak and Amy A Collins. 2003. Vibrotactile localization on the arm: Effects of place, space, and age. *Perception & psychophysics* 65, 7 (2003), 1058–1077.
- [11] Heather Culbertson, Cara M Nunez, Ali Israr, Frances Lau, Freddy Abnousi, and Allison M Okamura. 2018. A social haptic device to create continuous lateral motion using sequential normal indentation. In *2018 IEEE haptics symposium (HAPTICS)*. IEEE, 32–39.
- [12] Alexandra Delazio, Ken Nakagaki, Roberta L Klatzky, Scott E Hudson, Jill Fain Lehman, and Alanson P Sample. 2018. Force jacket: Pneumatically-actuated jacket for embodied haptic experiences. In *Proceedings of the 2018 CHI conference on human factors in computing systems*. 1–12.
- [13] Mihai Dragusanu, Alberto Villani, Domenico Prattichizzo, and Monica Malvezzi. 2021. Design of a wearable haptic device for hand palm cutaneous feedback. *Frontiers in Robotics and AI* 8 (2021), 706627.
- [14] Alberto Gallace, Hong Z Tan, and Charles Spence. 2007. The body surface as a communication system: The state of the art after 50 years. *Presence: Teleoperators and Virtual Environments* 16, 6 (2007), 655–676.
- [15] George A Gescheider. 1985. Psychophysics: Method, theory, and application. (*No Title*) (1985).
- [16] Sebastian Günther, Dominik Schön, Florian Müller, Max Mühlhäuser, and Martin Schmitz. 2020. PneumoVolley: Pressure-based haptic feedback on the head through pneumatic actuation. In *Extended Abstracts of the 2020 CHI Conference on Human Factors in Computing Systems*. 1–10.
- [17] Elisabet Henell, Judith Weda, Sophia Cedermalm, Linnéa Eklöv, Märta Häkansson, Jesper Nordström, Märit Reibring, Jonas Stålhund, Nils-Kristen Persson, Angelika Mader, et al. 2024. Pressure Stimuli and Spatiotemporal Illusions on the Forearm. *IEEE transactions on haptics* (2024).
- [18] Matthew J Hertenstein, Rachel Holmes, Margaret McCullough, and Dacher Keltner. 2009. The communication of emotion via touch. *Emotion* 9, 4 (2009), 566.
- [19] Ali Israr and Ivan Poupyrev. 2011. Tactile brush: drawing on skin with a tactile grid display. In *Proceedings of the SIGCHI Conference on Human Factors in Computing Systems*. 2019–2028.
- [20] Hiroo Iwata, Hiroaki Yano, Fumitaka Nakaizumi, and Ryo Kawamura. 2001. Project FEELEX: adding haptic surface to graphics. In *Proceedings of the 28th annual conference on Computer graphics and interactive techniques*. 469–476.
- [21] Soo-chan Jee and Myung Hwan Yun. 2016. An anthropometric survey of Korean hand and hand shape types. *International Journal of Industrial Ergonomics* 53 (2016), 10–18.
- [22] Minjae Jo, Dongkyu Kwak, and Sang Ho Yoon. 2023. WriMouCon: Wrist-mounted Haptic Controller for Rendering Physical Properties in Virtual Reality. In *2023 IEEE World Haptics Conference (WHC)*. IEEE, 34–40.
- [23] Kenneth O Johnson. 2001. The roles and functions of cutaneous mechanoreceptors. *Current opinion in neurobiology* 11, 4 (2001), 455–461.
- [24] Kenneth O Johnson and John R Phillips. 1981. Tactile spatial resolution. I. Two-point discrimination, gap detection, grating resolution, and letter recognition. *Journal of neurophysiology* 46, 6 (1981), 1177–1192.
- [25] Lynette A Jones and Susan J Lederman. 2006. *Human hand function*. Oxford university press.
- [26] Lynette A Jones and Hong Z Tan. 2012. Application of psychophysical techniques to haptic research. *IEEE transactions on haptics* 6, 3 (2012), 268–284.
- [27] Oliver Beren Kaul, Michael Rohs, Benjamin Simon, Kerem Can Demir, and Kamillo Ferry. 2020. Vibrotactile funneling illusion and localization performance on the head. In *Proceedings of the 2020 CHI Conference on Human Factors in Computing Systems*. 1–13.
- [28] Hamideh Kerdegari, Yeongmi Kim, Tom Stafford, and Tony J Prescott. 2014. Centralizing bias and the vibrotactile funneling illusion on the forehead. In *Haptics: Neuroscience, Devices, Modeling, and Applications: 9th International Conference, EuroHaptics 2014, Versailles, France, June 24–26, 2014, Proceedings, Part II* 9. Springer, 55–62.
- [29] Jinsoo Kim, Seungjae Oh, Chaeyong Park, and Seungmoon Choi. 2020. Body-penetrating tactile phantom sensations. In *Proceedings of the 2020 CHI Conference on Human Factors in Computing Systems*. 1–13.
- [30] Youngsun Kim, Jaedong Lee, and Gerard J. Kim. 2022. Designing of 2D Illusory Tactile Feedback for Hand-Held Tablets. In *Human-Computer Interaction – INTERACT 2015*. Springer-Verlag, Berlin, Heidelberg, 10–17. doi:10.1007/978-3-319-22723-8\_2

- [31] Sreela Kodali, Cihualpilli Camino Cruz, Thomas C Bulea, Kevin S Bharucha-Goebel, Alexander T Chesler, Carsten G Bonnemann, and Allison M Okamura. 2024. Spatial Summation of Localized Pressure for Haptic Sensory Prostheses. *arXiv preprint arXiv:2404.02565* (2024).
- [32] Lisheng Kuang, Marco Ferro, Monica Malvezzi, Domenico Prattichizzo, Paolo Robuffo Giordano, Francesco Chinello, and Claudio Pacchierotti. 2023. A wearable haptic device for the hand with interchangeable end-effectors. *IEEE Transactions on Haptics* (2023).
- [33] Lisheng Kuang, Monica Malvezzi, Domenico Prattichizzo, Paolo Robuffo Giordano, Francesco Chinello, and Claudio Pacchierotti. 2024. The HapticSpider: a 7-DoF Wearable Device for Cutaneous Interaction with the Palm. In *International Conference on Human Haptic Sensing and Touch Enabled Computer Applications*. Springer, 285–292.
- [34] Jean-Luc Lévêque, Johanna Dresler, Edith Ribot-Ciscar, Jean-Pierre Roll, and Christine Poelman. 2000. Changes in tactile spatial discrimination and cutaneous coding properties by skin hydration in the elderly. *Journal of investigative dermatology* 115, 3 (2000), 454–458.
- [35] HCCH Levitt. 1971. Transformed up-down methods in psychoacoustics. *The Journal of the Acoustical society of America* 49, 2B (1971), 467–477.
- [36] Bingxu Li and Gregory J Gerling. 2023. An individual's skin stiffness predicts their tactile discrimination of compliance. *The Journal of physiology* 601, 24 (2023), 5777–5794.
- [37] Xianglong Li, Tianjiao Zheng, Dongbao Sui, Nengxu Lin, Qinghua Zhang, Jie Zhao, and Yanhe Zhu. 2022. A 3D printed variable cross-section pneumatic soft manipulator with high-precision positioning capability: Design and control implementation. *Sensors and Actuators A: Physical* 342 (2022), 113644.
- [38] James C Makous, Robert M Friedman, and Charles J Vierck. 1995. A critical band filter in touch. *Journal of Neuroscience* 15, 4 (1995), 2808–2818.
- [39] Louise R Manfredi, Andrew T Baker, Damian O Elias, John F Dammann III, Mark C Zielinski, Vicky S Polashock, and Sliman J Bensmaia. 2012. The effect of surface wave propagation on neural responses to vibration in primate glabrous skin. *PLoS one* 7, 2 (2012), e31203.
- [40] Emese Nagy, Tibor Farkas, Frances Guy, and Anna Stafylarakis. 2020. Effects of handshake duration on other nonverbal behavior. *Perceptual and motor skills* 127, 1 (2020), 52–74.
- [41] Pierre-Henri Orefice, Mehdi Ammi, Moustapha Hafez, and Adriana Tapus. 2016. Let's handshake and I'll know who you are: Gender and personality discrimination in human-human and human-robot handshaking interaction. In *2016 IEEE-RAS 16th International Conference on Humanoid Robots (Humanoids)*. IEEE, 958–965.
- [42] Gunhyuk Park and Seungmoon Choi. 2018. Tactile information transmission by 2d stationary phantom sensations. In *Proceedings of the 2018 CHI conference on human factors in computing systems*. 1–12.
- [43] Jaeyoung Park, Jaeha Kim, Yonghwan Oh, and Hong Z Tan. 2016. Rendering moving tactile stroke on the palm using a sparse 2d array. In *Haptics: Perception, Devices, Control, and Applications: 10th International Conference, EuroHaptics 2016, London, UK, July 4–7, 2016, Proceedings, Part I 10*. Springer, 47–56.
- [44] Antonio Pérez-González, Margarita Vergara, and Joaquín L Sancho-Bru. 2013. Stiffness map of the grasping contact areas of the human hand. *Journal of biomechanics* 46, 15 (2013), 2644–2650.
- [45] Evan Pezent, Ali Israr, Majed Samad, Shea Robinson, Priyanshu Agarwal, Hrvoje Benko, and Nick Colonnese. 2019. Tasbi: Multisensory squeeze and vibrotactile wrist haptics for augmented and virtual reality. In *2019 IEEE World Haptics Conference (WHC)*. IEEE, 1–6.
- [46] Dale Purves, George J Augustine, David Fitzpatrick, Lawrence C Katz, Anthony-Samuel LaMantia, James O McNamara, S Mark Williams, et al. 2001. Mechanoreceptors specialized to receive tactile information. *Neuroscience* 9 (2001).
- [47] Saito Sakaguchi, Kaoru Saito, Naomi Arakawa, and Masashi Konyo. 2023. The dynamic behavior of skin in response to vibrating touch stimuli affects tactile perception. *Skin Research and Technology* 29, 3 (2023), e13295.
- [48] Niklas Schäfer, Julian Seiler, Bastian Latsch, Mario Kupnik, and Philipp Beckerle. 2025. Vibrotactile Phantom Sensations in Haptic Wrist Rotation Guidance. *IEEE Transactions on Haptics* (2025).
- [49] Senseglove. 2024. Nova2. <https://www.senseglove.com/product/nova-2/> Accessed: 2025-02-01.
- [50] Jongman Seo and Seungmoon Choi. 2010. Initial study for creating linearly moving vibrotactile sensation on mobile device. In *2010 IEEE Haptics Symposium*. IEEE, 67–70.
- [51] Jongman Seo and Seungmoon Choi. 2013. Perceptual analysis of vibrotactile flows on a mobile device. *IEEE transactions on haptics* 6, 4 (2013), 522–527.
- [52] Frederico M Severgnini, Juan S Martinez, Hong Z Tan, and Charlotte M Reed. 2021. Snake effect: A novel haptic illusion. *IEEE Transactions on Haptics* 14, 4 (2021), 907–913.
- [53] Yitian Shao, Vincent Hayward, and Yon Visell. 2016. Spatial patterns of cutaneous vibration during whole-hand haptic interactions. *Proceedings of the National Academy of Sciences* 113, 15 (2016), 4188–4193.
- [54] Vivian Shen, Tucker Rae-Grant, Joe Mullenbach, Chris Harrison, and Craig Shultz. 2023. Fluid reality: High-resolution, untethered haptic gloves using electroosmotic pump arrays. In *Proceedings of the 36th Annual ACM Symposium on User Interface Software and Technology*. 1–20.

- [55] Craig Shultz and Chris Harrison. 2023. Flat panel haptics: Embedded electroosmotic pumps for scalable shape displays. In *Proceedings of the 2023 CHI conference on human factors in computing systems*. 1–16.
- [56] Youjin Sung, Rachel Kim, Kun Woo Song, Yitian Shao, and Sang Ho Yoon. 2024. Hapticilot: Authoring in-situ hand posture-adaptive vibrotactile feedback for virtual reality. *Proceedings of the ACM on Interactive, Mobile, Wearable and Ubiquitous Technologies* 7, 4 (2024), 1–28.
- [57] Hong Z Tan, Mandayam A Srinivasan, Brian Eberman, and Belinda Cheng. 1994. Human factors for the design of force-reflecting haptic interfaces. *Dynamic Systems and Control* 55, 1 (1994), 353–359.
- [58] Jonathan Tong, Oliver Mao, and Daniel Goldreich. 2013. Two-point orientation discrimination versus the traditional two-point test for tactile spatial acuity assessment. *Frontiers in human neuroscience* 7 (2013), 579.
- [59] Qianqian Tong, Wenxuan Wei, Yuan Guo, Tianhao Jin, Ziqi Wang, Hongxing Zhang, Yuru Zhang, and Dangxiao Wang. 2024. Distant handshakes: Conveying social intentions through multi-modal soft haptic gloves. *IEEE Transactions on Affective Computing* (2024).
- [60] Daria Trinitatova and Dzmitry Tsetserukou. 2019. Deltatouch: a 3d haptic display for delivering multimodal tactile stimuli at the palm. In *2019 IEEE World Haptics Conference (WHC)*. IEEE, 73–78.
- [61] G v. Békésy. 1958. Funneling in the nervous system and its role in loudness and sensation intensity on the skin. *The Journal of the Acoustical Society of America* 30, 5 (1958), 399–412.
- [62] Robert W Van Boven and Kenneth O Johnson. 1994. The limit of tactile spatial resolution in humans: grating orientation discrimination at the lip, tongue, and finger. *Neurology* 44, 12 (1994), 2361–2361.
- [63] Georg Von Békésy. 1959. Neural funneling along the skin and between the inner and outer hair cells of the cochlea. *The Journal of the Acoustical Society of America* 31, 9 (1959), 1236–1249.
- [64] Shun Watatami, Hikaru Nagano, Yuichi Tazaki, and Yasuyoshi Yokokohji. 2025. Tele Haptic Handshake Using Distributed Pressure Presentation Device and Mutual Interaction Pressure Model. *Electronics* 14, 3 (2025), 537.
- [65] Ernst Heinrich Weber. 1996. *EH Weber on the tactile senses*. Psychology Press.
- [66] Weicheng Wu and Heather Culbertson. 2019. Wearable haptic pneumatic device for creating the illusion of lateral motion on the arm. In *2019 IEEE World Haptics Conference (WHC)*. IEEE, 193–198.
- [67] Seiya Yamaguchi, Takefumi Hiraki, Hiroki Ishizuka, and Norihisa Miki. 2023. Handshake feedback in a haptic glove using pouch actuators. In *Actuators*, Vol. 12. MDPI, 51.
- [68] Xingyu Yang and Kening Zhu. 2023. Emoband: Investigating the affective perception towards on-wrist stroking and squeezing feedback mediated by different textile materials. In *Proceedings of the 2023 CHI conference on human factors in computing systems*. 1–20.
- [69] Shigeo Yoshida, Yuqian Sun, and Hideaki Kuzuoka. 2020. Pocopo: Handheld pin-based shape display for haptic rendering in virtual reality. In *Proceedings of the 2020 CHI Conference on Human Factors in Computing Systems*. 1–13.
- [70] Gyeore Yun, Seungjae Oh, and Seungmoon Choi. 2019. Seamless phantom sensation moving across a wide range of body. In *2019 IEEE world haptics conference (WHC)*. IEEE, 616–621.
- [71] Mengjia Zhu, Amirhossein H Memar, Aakar Gupta, Majed Samad, Priyanshu Agarwal, Yon Visell, Sean J Keller, and Nicholas Colonnese. 2020. Pneusleeve: In-fabric multimodal actuation and sensing in a soft, compact, and expressive haptic sleeve. In *Proceedings of the 2020 CHI conference on human factors in computing systems*. 1–12.